

Copyright WILEY-VCH Verlag GmbH & Co. KGaA, 69469 Weinheim, Germany, 2014.

ADVANCED FUNCTIONAL MATERIALS

Supporting Information

for *Adv. Funct. Mater.*, DOI: 10.1002/adfm.201400494

Surface Textured Polymer Fibers for Microfluidics

*Adem Yildirim, Muhammad Yunusa, Fahri Emre Ozturk,
Mehmet Kanik, and Mehmet Bayindir**

SUPPORTING INFORMATION

Surface Textured Polymer Fibers for Microfluidics

By Adem Yildirim, Muhammad Yunusa, Fahri Emre Ozturk, Mehmet Kanik and Mehmet Bayindir*

Prof. M. Bayindir, Adem Yildirim, Muhammad Yunusa, Fahri Emre Ozturk, Mehmet Kanik
UNAM-National Nanotechnology Research Center and Institute of Materials Science and
Nanotechnology, Bilkent University, 06800 Ankara, Turkey
E-mail: bayindir@nano.org.tr

Prof. M. Bayindir
Department of Physics, Bilkent University, 06800 Ankara, Turkey

Keywords: *microfluidics, anisotropic wetting, polymer fiber drawing, capillary flow, colorimetric protein assay*

We have provided spontaneous capillary flow calculation in grooved fibers, SEM images of the smooth fiber (Figure S1), UV-Vis and FTIR spectra of PDA (Figures S2 and S3 and Table 1) water spreading on uncoated star-shaped and PDA coated smooth fibers (Figure S4), water contact angles of bare and PDA coated PEI films (Figure S5), analysis of array filling time depending on fiber size, array length and shape (Figures S6 and S7), additional examples of fiber based microfluidic channel geometries (Figures S8 and S9), and additional results for protein assay (Table 2 and Figures S10 and S11).

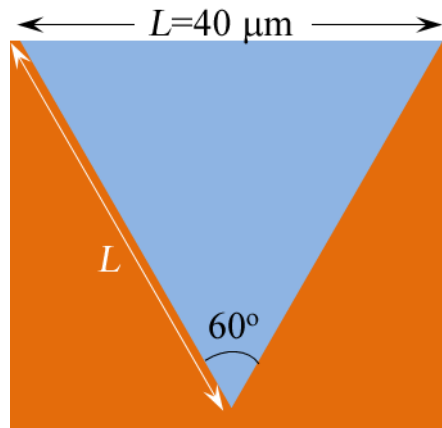
S1. Spontaneous capillary flow calculation

The spontaneous capillary flow equation (Eq. S1) is applied on equilateral triangle groove geometry of star-shaped fibers.^[1] Scheme S1 shows a groove of 300 μm diameter fiber filled with water. The ratio of free perimeter (liquid air contact line length) P_f to wet perimeter (liquid solid contact line length) P_w gives the contact angle limit for spontaneous wetting (*i.e.* contact angle value of the smooth surfaced material that would allow spontaneous wetting at the studied geometry).

$$\frac{P_f}{P_w} < \cos \theta \quad (\text{Eq. S1})$$

$$\frac{P_f}{P_w} = \frac{L}{2L} \quad (\text{Eq. S2})$$

$$\theta < 60^\circ \quad (\text{Eq. S3})$$



Scheme S1. Geometry of a single groove on a 300 μm diameter fiber filled with water. The groove is an equilateral triangle of side length 40 μm .

Increased hydrophobicity is observed at uncoated star-shaped fibers. This is due to increased roughness of the hydrophobic PEI surface (PEI film has a contact angle of 97°). After PDA coating of the PEI film however, contact angle value decreases to 32° (which is below the calculated limit of 60° for groove geometry) and spontaneous flow is observed within the grooves. Equation S1 helps us to understand contribution of micro-grooves to observe extreme anisotropic wetting properties of star-shaped fibers.

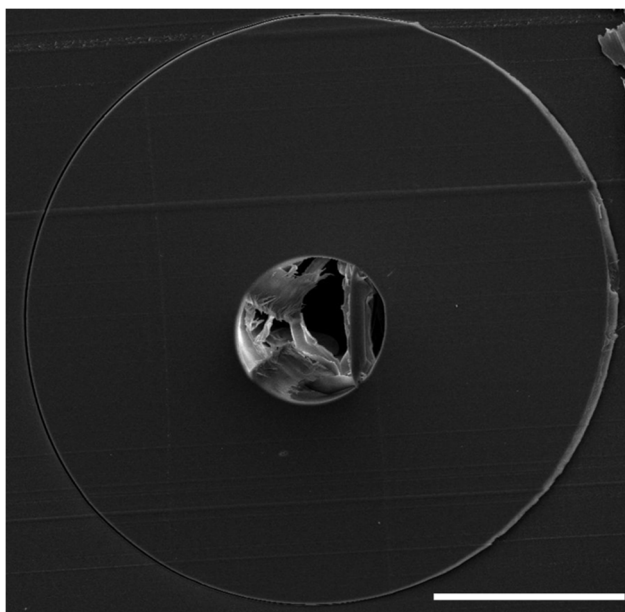
S2. Characterization of smooth fibers

Figure S1. Cross-sectional SEM image of smooth PEI fiber with a diameter of 300 μm . (Scale bar: 100 μm).

S3. Chemical characterization of PDA

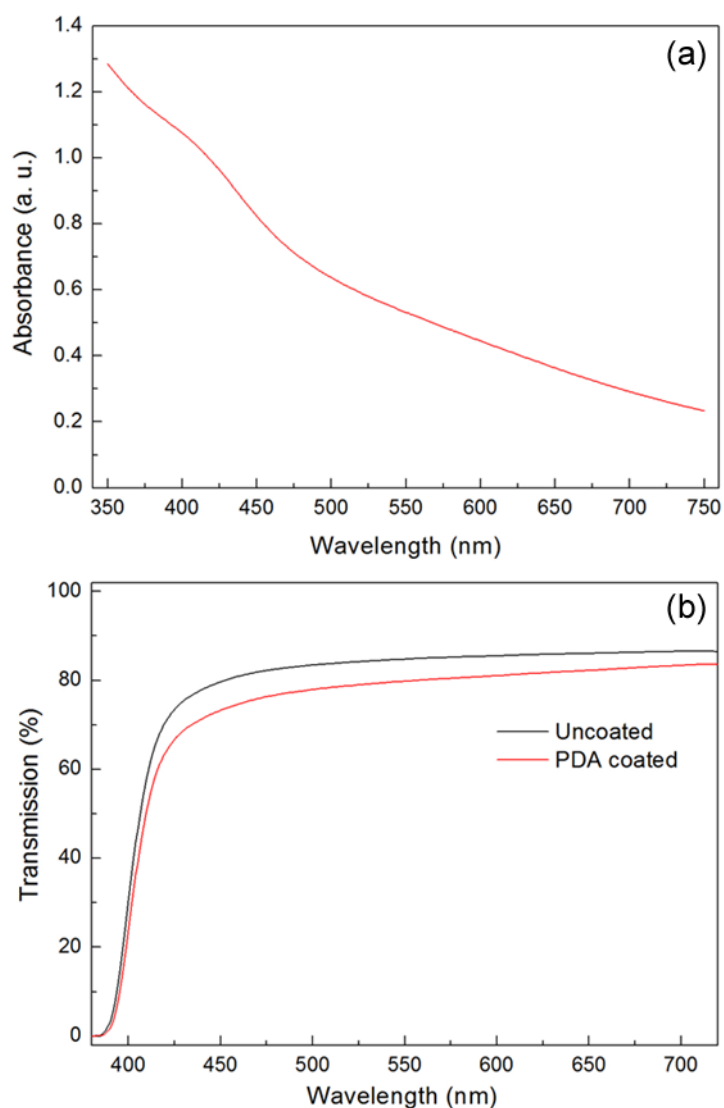


Figure S2. (a) Absorption spectrum of dopamine solution, which is polymerized for 24 hours, showing the broad absorption of PDA. (b) Transmission spectra of PDA coated and bare PEI film. Film transmission decreased after PDA deposition.

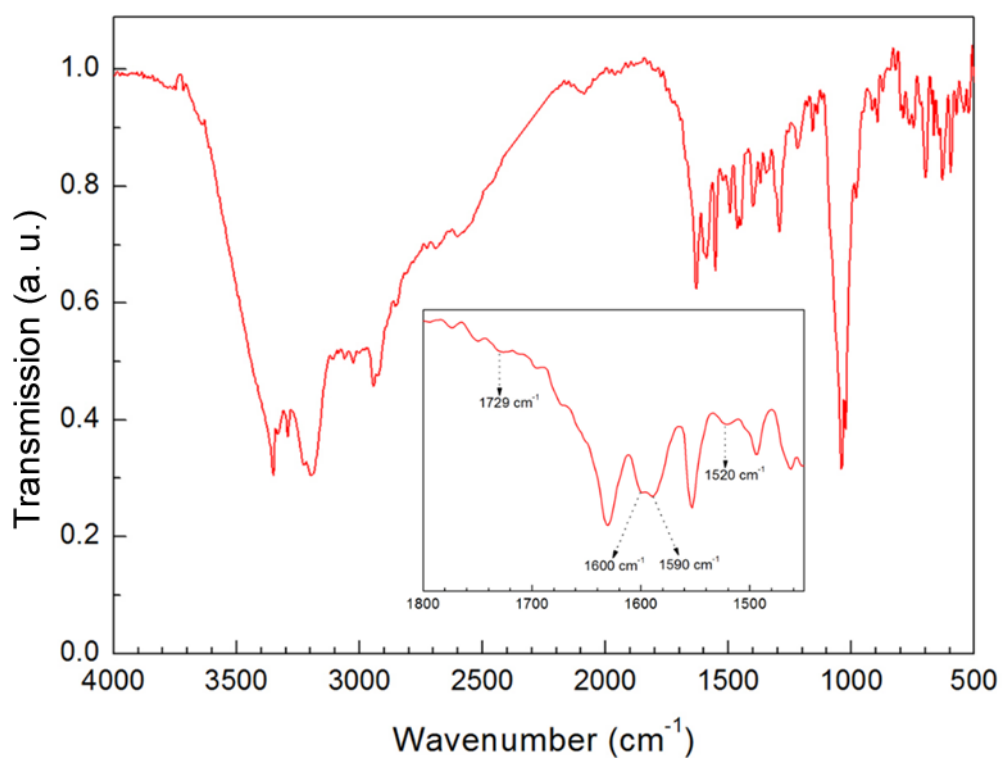


Figure S3. FTIR spectrum of PDA powder, which is polymerized for 24 hours. Inset shows the assigned peaks.

Table S1. Infrared bands of PDA powder

Wavenumber (cm ⁻¹)	Assignment
3000 - 3500 broad	$\nu(\text{O-H}), \nu(\text{N-H})$
1728 weak, shoulder	$\nu(\text{C=O})$
1600	$\nu_{\text{ring}}(\text{C-N})$
1590	$\nu_{\text{ring}}(\text{C=C})$
1520 weak	$\nu_{\text{ring}}(\text{C=N})$

S4. Additional images for single fibers and PEI films

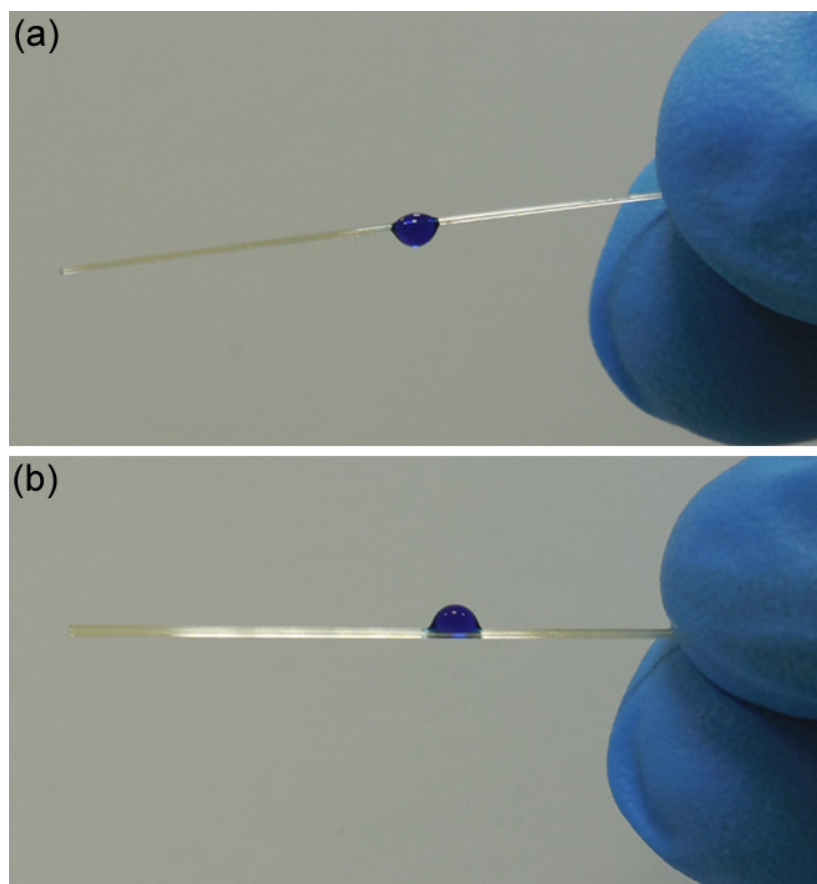


Figure S4. Colored water droplets (3 μL) on (a) PDA coated smooth and (b) uncoated star-shaped fibers, indicating that for complete wetting of fiber surface both grooved structure and PDA coating is essential.

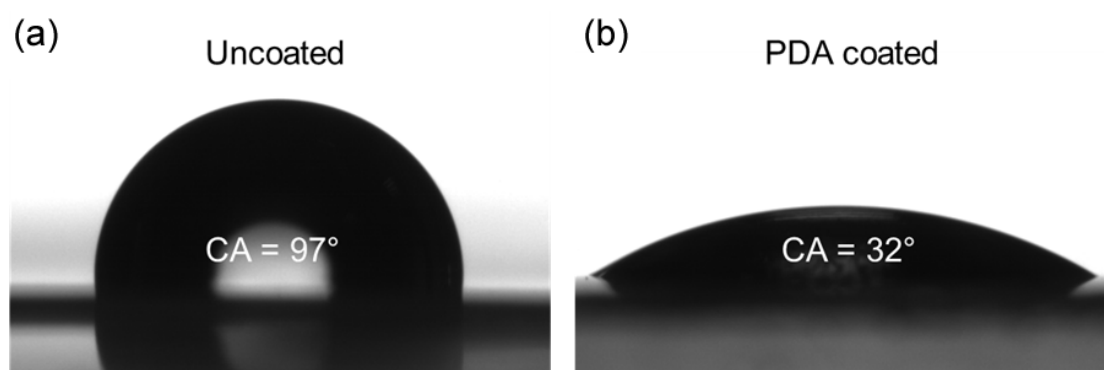


Figure S5. Water contact angles (CA) of bare PEI (a) and PDA coated (b) PEI films. After modification with PDA hydrophobic polymer surface becomes very hydrophilic.

S5. Water spreading dynamics of fiber arrays

The rate of capillary wicking in cylindrical geometries can be explained with Washburn's law.^[2] Washburn's model estimates wicking distance to be proportional with the square root of time. The triangular groove geometry of the fibers in this study are not consistent with the assumptions under which Washburn's law is derived. Additionally, the model takes only closed-channels into consideration; either single cylindrical channels or porous bodies, therefore it would not apply for open-channel groove geometry of the fibers in this study.

However, a similar approach to open triangular geometry of the grooves yields results perfectly analogous to Washburn's equation.^[3,4] In the case of spreading to a triangular groove from a reservoir, the height of the liquid in the groove is approximated to be constant and the relationship between spreading distance and time is described with a square root law. Experiments with various liquids demonstrated that spreading distance L is accurately proportional to square root of time \sqrt{t} for open triangular geometries.^[4,5]

To see if these arguments hold for an array of star-shaped fibers, we measured spreading of liquid versus time for arrays of 500 μm , 300 μm , and 200 μm star-shaped fibers. Dyed water was introduced to the array from one end, and video of the liquid spreading was recorded with a standard digital camera (Nikon Coolpix S6400). Then the position of liquid front was measured and plotted as a function of square root of time (Figure S6). On each of the three arrays, there is a linear relationship between L and \sqrt{t} with R^2 values larger than 0.99. Therefore, spreading in star-shaped fibers agree well with previously described models for triangular grooves. Further, spreading speed increases with increasing fiber diameter (thus with increasing side lengths of equilateral triangle grooves), which is also consistent with previous reports.^[3-5]

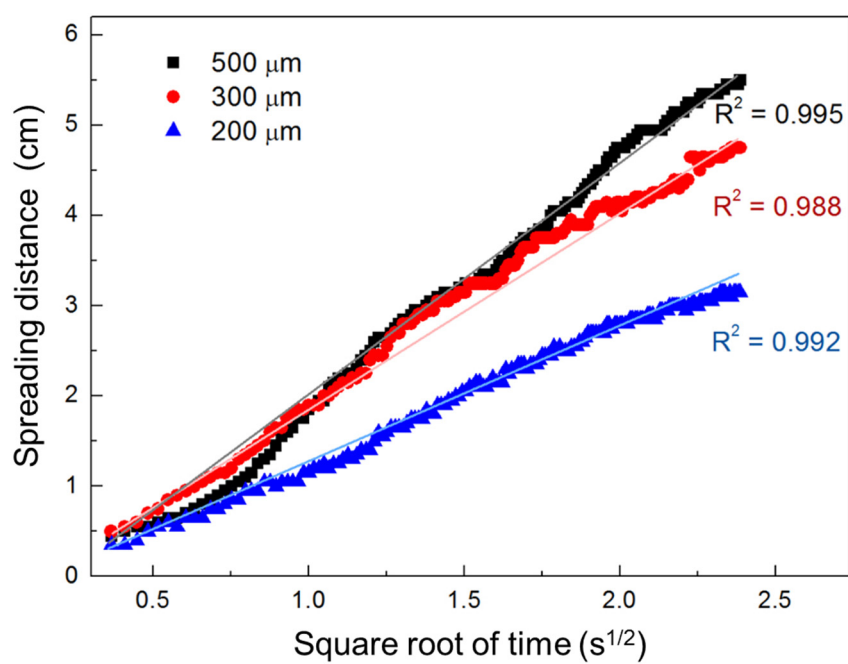


Figure S6. Spreading rates in fiber arrays with various fiber diameters (500 μm, 300 μm, and 200 μm).

S6. Effects of channel length and shape on channel filling time

In order to investigate the effect of different parameter on channel filling time, we prepared four different surfaces; a 5 cm long straight fiber array, a 10 cm long straight fiber array, a 10 cm long curved fiber array with two turns, and a 15 cm long curved fiber array with four turns. We measured the water filling times of straight fiber arrays (5 and 10 cm), curved fiber array with two turns (10 cm), and curved fiber array with four turns (15 cm), which are 7 seconds, 16 seconds, 35 seconds and 2.5 minutes, respectively (Figure S7). Based on these results, we can conclude that depending on the fiber length and array shape array filling time might change from a few seconds to a few minutes. In general, with the increasing fiber length, the number of bends, and curvature radius of bends, filling time increases significantly.

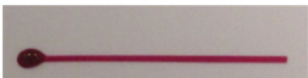

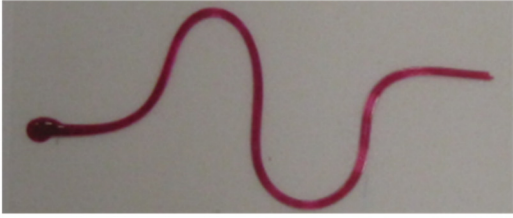
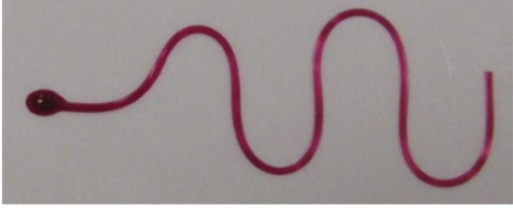
Array		Filling Time (s)
5 cm straight		7
10 cm straight		16
10 cm curved		35
15 cm curved		150

Figure S7. Water, 20 μ L, filling times of four different open microfluidic channels.

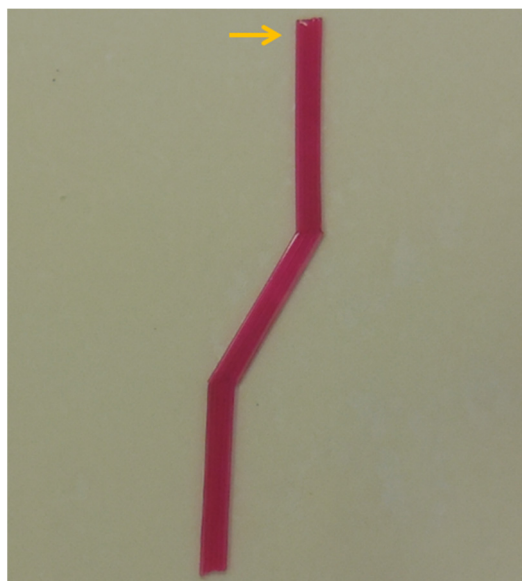
S7. Additional images for fiber arrays

Figure S8. Demonstration of end to end added channels that can transmit water from one to another. Orange arrow shows the point of dyed water introduction.

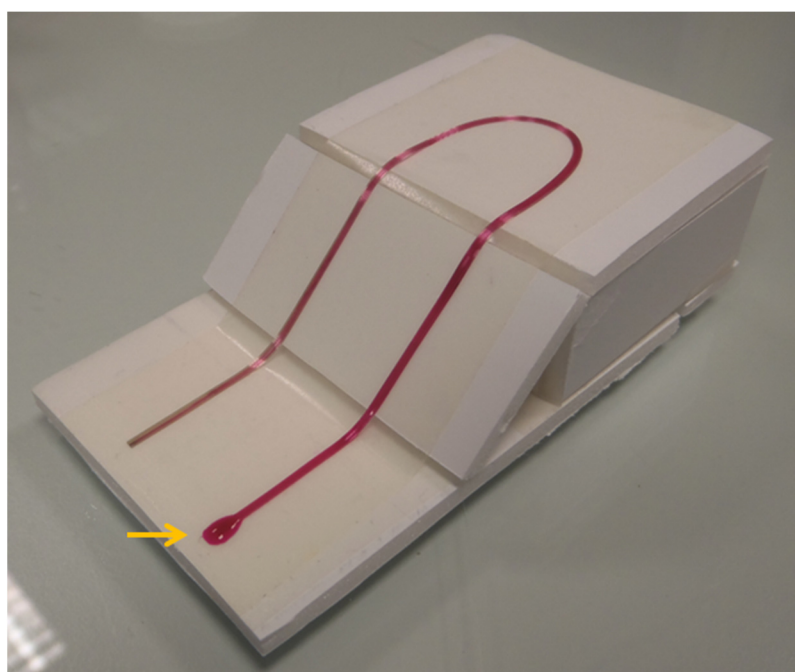


Figure S9. An example of a microfluidic channel demonstration on a three-dimensional object which shows fluid climbing a ramp. Orange arrow shows the point of dyed water introduction.

S8. Additional data for protein assay

Table S1. RGB (Red, green and blue) values collected for 10 individual pixels for each analysis and control spot. RGB color model assigns a numerical value to each of the three primary colors, red, green and blue, in order to define each possible color as a function of the primary colors. The yellow shade of analysis spots and the blue shade of control spots were captured by a conventional scanner and RGB values were extracted by a commercial image editing software.

Analysis1	R	G	B	Analysis2	R	G	B	Analysis3	R	G	B
Pixel #1	237	242	201	Pixel #1	231	232	162	Pixel #1	214	224	189
Pixel #2	233	239	229	Pixel #2	226	233	200	Pixel #2	219	232	225
Pixel #3	212	230	242	Pixel #3	210	226	215	Pixel #3	213	230	237
Pixel #4	212	231	245	Pixel #4	202	221	228	Pixel #4	207	225	239
Pixel #5	210	228	252	Pixel #5	194	220	237	Pixel #5	202	227	247
Pixel #6	212	227	255	Pixel #6	211	219	255	Pixel #6	201	223	246
Pixel #7	223	240	250	Pixel #7	201	224	238	Pixel #7	201	222	241
Pixel #8	212	230	242	Pixel #8	206	221	228	Pixel #8	213	230	237
Pixel #9	214	234	245	Pixel #9	209	231	244	Pixel #9	201	220	235
Pixel #10	213	224	246	Pixel #10	207	234	251	Pixel #10	191	217	250
Control1	R	G	B	Control2	R	G	B	Control3	R	G	B
Pixel #1	254	253	248	Pixel #1	250	250	198	Pixel #1	249	250	242
Pixel #2	255	255	250	Pixel #2	254	253	205	Pixel #2	252	254	232
Pixel #3	254	253	223	Pixel #3	253	247	197	Pixel #3	254	255	237
Pixel #4	254	254	220	Pixel #4	250	238	188	Pixel #4	253	250	215
Pixel #5	254	250	221	Pixel #5	245	237	188	Pixel #5	254	254	220
Pixel #6	254	250	221	Pixel #6	253	254	214	Pixel #6	254	253	223
Pixel #7	255	255	234	Pixel #7	254	249	207	Pixel #7	255	255	231
Pixel #8	255	255	229	Pixel #8	255	250	202	Pixel #8	255	255	231
Pixel #9	254	254	216	Pixel #9	255	250	212	Pixel #9	254	252	227
Pixel#10	245	241	206	Pixel#10	255	253	214	Pixel#10	253	255	233

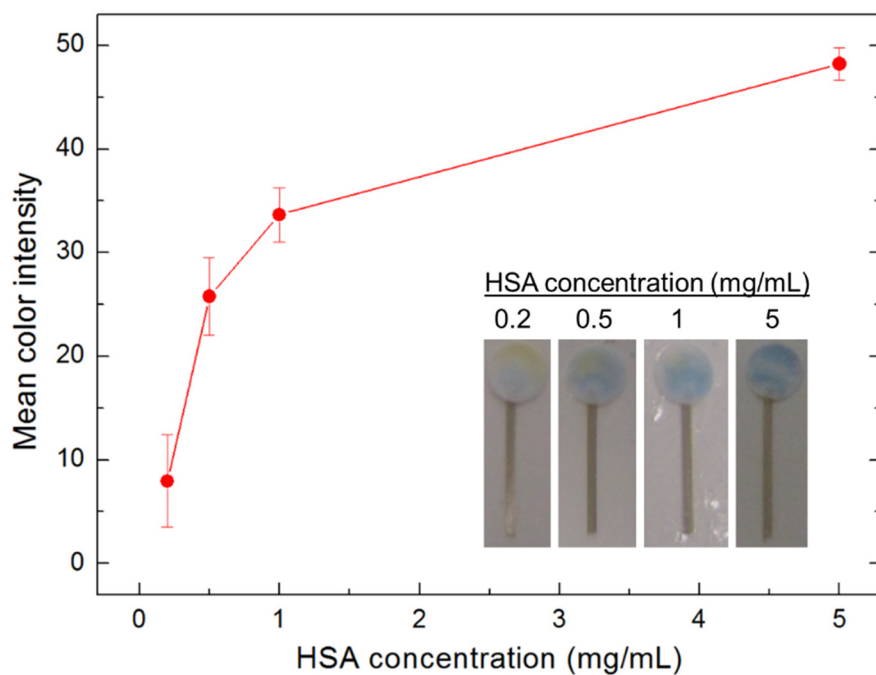


Figure S10. Concentration dependent colorimetric response of the array. All experiments were performed in triplicate. Mean color intensities were calculated by averaging the change in the RGB values (compared to white) of randomly selected pixels. Inset shows the photographs of the color change in the assays after protein introduction.

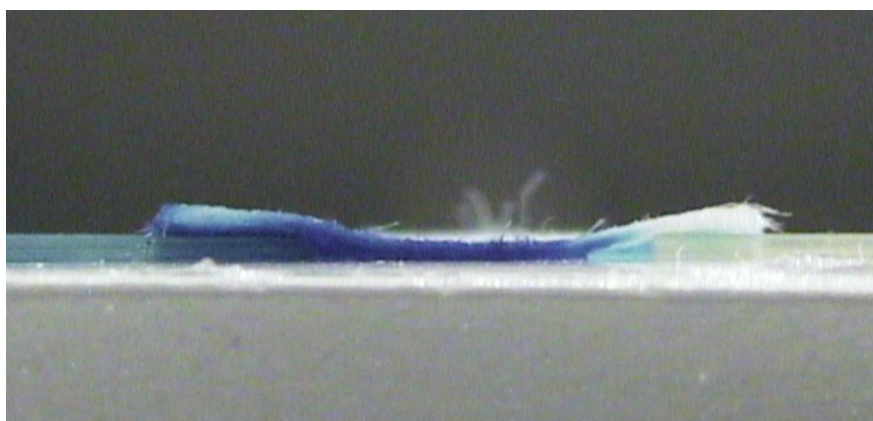


Figure S11. Side view of a gap covered with a piece of paper, similar to the control spots in the protein assay. Although the two channels are connected over the gap with a piece of paper, blue colored water (introduced to the channel at left) did not transfer to the other channel (right channel).

References

- [1] B. P. Casavanta, E. Berthier, A. B. Theberge, J. Berthier, S. I. Montanez-Sauri, L. L. Bischel, K. Brakke, C. J. Hedman, W. Bushman, N. P. Keller, and David J. Beebe, Suspended microfluidics. *Proc. Natl. Acad. Sci. USA* **2013**, *110*, 10111.
- [2] E. W. Washburn, The dynamics of capillary flow. *Phys. Rev.* **1921**, *17*, 273.
- [3] P. B. Warren, Late stage kinetics for various wicking and spreading problems. *Phys. Rev. E.* **2004**, *69*, 041601.
- [4] J. A. Mann Jr., L. Romero, R. R. Rye, F. G. Yost, Flow of simple liquids down narrow V grooves. *Phys. Rev. E.* **1995**, *52*, 3967.
- [5] J. Tian, D. Kannangara, X. Lia, W. Shen, Capillary driven low-cost V-groove microfluidic device with high sample transport efficiency. *Lab Chip*, **2010**, *10*, 2258.